The fiber knob protein of human adenovirus type 49 mediates highly efficient and promiscuous infection of cancer cell lines using a novel cell entry mechanism

Alexander T. Baker[1,2], Gareth Marlow[1], James A. Davies[1], Elise Moses[1], Rosie M. Mundy[1], David K. Cole[3], Pierre J. Rizkallah[3], Alan L. Parker[1*]

[1]Division of Cancer and Genetics, School of Medicine, Cardiff University, Heath Park, Cardiff, CF14 4XN, UK.
[2]Current address: Department of Haematology and Oncology, Mayo Clinic, 13208 E Shea Blvd, Scottsdale, Arizona, 85259, USA
[3]Division of Infection and Immunity, School of Medicine, Cardiff University, Heath Park, Cardiff, CF14 4XN, UK.
*Corresponding Author, ParkerAL@Cardiff.ac.uk

Correspondence:
Dr Alan Parker
Division of Cancer and Genetics
Cardiff University
Heath Park
Cardiff
CF14 4XN
Telephone: +44 2922 510 231
Email: ParkerAL@cardiff.ac.uk

Word count
Abstract: 249
Importance: 150
Main text: 4638
Figure legends: 929
Figure count: 8 Figures (+1 Supplementary Table & 3 Supplementary Figures)

Running title: Ad49 fiber knob permits promiscuous cell entry

Abstract

The human adenovirus (HAdV) phylogenetic tree is diverse, divided across seven species and comprising over 100 individual types. Species D HAdV are rarely isolated with low rates of pre-existing immunity, making them appealing for therapeutic applications. Several species D vectors have been developed as vaccines against infectious diseases where they induce robust immunity in pre-clinical models and early phase clinical trials. However, many aspects of the basic virology of species D HAdV, including their basic receptor usage and means of cell entry, remain understudied.

Here, we investigated HAdV-D49, which previously has been studied for vaccine and vascular gene transfer applications. We generated a pseudotyped HAdV-C5 presenting the HAdV-D49 fiber knob protein (HAdV-C5/D49K). This pseudotyped vector was efficient at infecting cells devoid of all known HAdV receptors, indicating HAdV-D49 uses an unidentified cellular receptor. Conversely, a pseudotyped vector presenting the fiber knob protein of the closely related HAdV-D30 (HAdV-C5/D30K), differing in just four amino acids from HAdV-D49, failed to demonstrate the same tropism. These four amino acid changes resulted in a change in isoelectric point of the knob protein, with HAdV-D49K presenting a highly basic region around the apex compared to HAdV-D30K. Structurally and biologically we demonstrate that HAdV-D49 knob protein is unable to engage CD46, whilst potential interaction with CAR is extremely limited by extension of the DG loop. HAdV-C5/49K efficiently transduced cancer cell lines of pancreatic, breast, lung, oesophageal and ovarian origin, indicating it may have potential for oncolytic virotherapy applications, especially for difficult to transduce tumour types.

54 ## Importance

55 Adenoviruses are powerful tools experimentally and clinically. To maximise efficacy, the development of
56 serotypes with low levels of pre-existing immunity in the population is desirable. Consequently,
57 attention has focussed on those derived from species D, which have proven robust vaccine platforms.
58 This widespread usage is despite limited knowledge underpinning their basic biology and cellular
59 tropism.

60 We investigated the tropism of HAdV-D49, demonstrating it uses a novel cell entry mechanism that
61 bypasses all known HAdV receptors. We demonstrate, biologically, that a pseudotyped HAdV-C5/D49K
62 vector efficiently transduces a wide range of cell lines, including those presenting no known adenovirus
63 receptor. Structural investigation suggests that this broad tropism is the result of a highly basic surface
64 electrostatic potential, since a homologous pseudotyped vector with a more acidic surface potential,
65 HAdV-C5/D30K, does not have a similar pan-tropism. Therefore, HAdV-C5/D49K may form a powerful
66 vector for therapeutic applications capable of infecting difficult to transduce cells.

67 # Introduction:

68 Human adenoviruses are divided into seven species, A-G[1]. These non-enveloped, icosahedral viruses
69 have garnered significant interest as therapeutic vectors where they can be grown and purified to high
70 titers, and where the double-stranded DNA genome is readily amenable to genetic modification to
71 enable the overexpression of therapeutic transgenes[2,3]. Similar techniques can also be applied to
72 genetically alter the virus structural genes, creating modified virus tropisms which are retained by
73 progeny virions after replication.

74 Clinically, adenoviruses have been developed as vectors for gene therapy, vaccines, and as oncolytic
75 virotherapies[1,4,5]. However, all these applications can be hampered by pre-existing immunity against the
76 therapeutic vector in the population resulting from prior exposure to the wild type pathogen. Such pre-
77 existing immunity is likely to reduce the therapeutic index of such systems, due to rapid and efficient
78 removal of the engineered therapeutic agent by the reticuloendothelial system[6,7]. This is especially
79 relevant where the therapeutic is based on the most commonly studied species C adenovirus, human
80 adenovirus type 5 (HAdV-C5), where neutralising antibodies are found in ~90% of patients from sub-
81 Saharan Africa and ~30% of a Scottish patient cohort[8,9].

82 A promising means to circumvent pre-existing immunity is through the development of viruses with
83 naturally low seroprevalence rates as therapeutic agents. For example, vaccines have been developed
84 using chimpanzee adenoviruses which have little to no seroprevalence in humans. However, it appears a
85 significant percentage of the population may still harbour some immunity to chimpanzee adenoviruses,
86 as observed in a cohort from China[10].

87 Most attempts to develop adenoviruses with low seroprevalence have focused on those derived from
88 species B or D, due to their comparative rarity[5,9,11]. The most clinically advanced of these are HAdV-D26
89 and Enadenotucirev (formerly ColoAd1)[12]. Enadenotucirev was developed by evolution of a panel of

90 different adenovirus strains to select for recombinants with rapid replication in tumour cell. The
91 resultant selected recombinant was predominantly HAdV-B11 with some elements of HAdV-B3, and has
92 progressed into clinical trials as a cancer therapeutic[13,14]. HAdV-D26, is a replication deficient vector and
93 the basis of the Ad26.ZEBOV vaccine against Ebola virus, currently under evaluation in the PREVAIL and
94 PREVAC studies[15,16].

95 Many species D adenoviruses have previously been evaluated for their potential as vaccines, gene
96 therapies, and oncolytic viruses[1,5,9,11]. One with particularly low seroprevalence rates is HAdV-D49. In a
97 cohort of 100 Belgian individuals only 2% had HAdV-D49 positive sera, whilst no pre-existing immunity
98 against HAdV-D49 was detected in 103 Scottish patients[8,17]. Prevalence is somewhat higher in sub-
99 saharan Africa with 22% of 200 patients presenting neutralising antibodies (nAbs), highlighting
100 significant geographical variation in seroprevelance[9].

101 HAdV-D49 was first isolated from the faeces of a human with no observed disease, and later from Dutch
102 patients[18,19]. It was then isolated from nosocomial epidemic keratoconjunctivitis infections[20,21], but is
103 most associated with patients who are immunocompromised due to HIV infection[22]. A study of
104 adenovirus infections in patients from the UK and Netherlands found 11 instances of HAdV-D49
105 infection in 183 HIV positive patients (6% HAdV-D49 positive), compared to just two instances in 2301
106 tested healthy patients (0.09% HAdV-D49 positive)[19].

107 Previous studies suggest that HAdV-D49 may be effective as a vaccine vector. A vaccine vector based on
108 HAdV-D49 has been evaluated previously for its ability to protect against simian immunodeficiency virus
109 challenge. This vector induced strong anti-SIVGag $CD8^+$ mediated immunity to SIV, greater than the
110 comparable HAdV-C5 based vector[23]. Another study sought to exploit HAdV-D49 a gene therapy to
111 reduce excessive cell smooth muscle proliferation in vascular conduits following bypass grafting. This
112 study demonstrated that HAdV-D49 was efficient at infecting endothelial cells and vascular smooth

113 muscle cells, even after short exposure times[8]. Studies in CAR, CD46, and α2-3 linked sialic acid
114 expressing cells suggest HAdV-D49 may engage CD46 as a cellular receptor, although the effects
115 observed were small[23].

116 Despite these studies and the development of HAdV-D49 as a therapeutic agent, there remains little
117 information surrounding the basic biology of HAdV-D49 and its means of cellular engagement. Here, we
118 structurally and functionally investigate the tropism of HAdV-D49, focussing on the fiber knob protein as
119 the major mediator of cellular attachment, and evaluate the potential utility of a pseudotyped HAdV-
120 C5/D49K vector to infect a range of cancer cell lines.

121 # Results and Discussion

122 ## HAdV-C5/D49K is not dependent on any known adenovirus receptor for cell entry

123 To investigate the receptor usage of human adenovirus type 49 fiber knob protein we created a
124 replication incompetent HAdV-C5 vector pseudotyped with the fiber knob protein of HAdV-D49 (HAdV-
125 C5/D49K), expressing a green fluorescent protein (GFP) transgene. This is a well-established means to
126 investigate the fiber knob in the context of a well understood, replication incompetent virus[1,24]. Using
127 this pseudotyped vector, we performed transduction assays in CHO cells expressing common adenovirus
128 receptors (Figure 1). CHO-K1 cells do not express any known adenovirus receptors. CHO-CAR cells are
129 express the HAdV-C5 receptor coxsackie and adenovirus receptor (CAR), whilst CHO-BC1 cells have been
130 express the BC1 isoform of CD46, the major receptor for species BI which includes HAdV-B35.

131 We compared the transduction of HAdV-C5/D49K to similar GFP expressing replication incompetent
132 vectors HAdV-C5 and HAdV-C5/B35K, which utilise CAR and CD46 as receptors, respectively[24–26]. As
133 expected, HAdV-C5/D35K was unable to transduce CHO-CAR efficiently, due to the lack of CD46, whilst
134 HAdV-C5 transduced them with high efficiency, due to the presence of CAR. HAdV-C5/D49K transduced
135 CHO-CAR cells efficiently, but slightly less efficiently (by ~20%) compared to HAdV-C5 (Figure 1A). In
136 CHO-BC1 cells HAdV-C5 was inefficient, due to the lack of CAR expression, whilst HAdV-C5/B35
137 transduced with almost 100% efficiency, due to the presence of high affinity HAdV-B35 receptor, CD46.

138 HAdV-C5/D49K demonstrated similar ability to HAdV-C5-B35K to transduce CHO-BC1 cells (Figure 1B). In
139 CHO-K1 cells neither HAdV-C5 nor HAdV-C5/B35K were able to efficiently transduce the cells due to the
140 lack of a suitable cell surface receptor. HAdV-C5/D49K, however, transduced these cells highly
141 efficiently, indicating that HAdV-D49K is able to infect cells efficiently and independently of CAR or CD46
142 (Figure 1C), thus indicating that HAdVC5/D49K engages an alternative cellular receptor. Interestingly, we

143 also observed, in this and later experiments, that HAdV-C5/D49K is somewhat less efficient at infecting
144 CHO-CAR cells (Figure 1A) compared to non-CAR expressing CHO cell types (Figure 1B-C). These data
145 indicating the that presence of CAR may actively reduce the transduction efficiency of HAdVC5/D49K
146 compared to levels of transduction in the absence of CAR in the same cell line background.

147 We performed similar transduction assays in CHO-K1 and SKOV-3 ovarian cancer cells with and without
148 pre-treatment with either Heparinase or Neuraminidase to determine the ability of HAdVC5/D49K to
149 engage heparan sulphate proteoglycans (HSPGs) or sialic acid, respectively, to mediate cellular infection
150 (Figure 2). As a positive control for heparinase activity we compared HAdV-C5/D49K infectivity to that of
151 HAdV-C5 in the presence and absence of FX[27]. We observed in CHO-K1 and SKOV-3 cells that
152 transduction levels of HAdV-C5 alone were poor (Figure 2A, B), but were significantly enhanced by the
153 presence of FX, enabling engagement of heparan sulphate proteoglycans (HSPGs) via "FX-bridging" the
154 hexon protein[28–30]. Treatment with heparinase to cleave cellular HSPGs reduced transduction efficiency
155 back to that of HAdV-C5 alone. HAdV-C5/D49K transduction efficiency was unaffected by treatment with
156 heparinase (Figure 2A, B), indicating that HAdV-D49 is unlikely to utilise HSPGs for cell entry.

157 Treatment with neuraminidase to remove cellular sialic acid did not affect the ability of any of the
158 viruses to transduce CHO-K1 cells (Figure 2C), as we previously demonstrated to show the involvement
159 of sialic acid in HAdV-C5/D26K infection[24]. In SKOV-3 cells, removal of sialic acid enhanced the
160 transduction mediated by HAdV-C5/D49K and HAdV-C5/B35K, an effect which we have previously
161 observed by neuraminidase treatment in SKOV-3 cells (Figure 2D)[24,31,32]. This effect could be a result of
162 the removal of sialic acid, enhancing non-specific charge based interactions between the cell surface and
163 viral capsid. Regardless, these data do not support a role for sialic acid in HAdV-C5/D49K cell infection.

164 The transduction affinity of HAdV-C5/D49K in the experiments in Figure 2 was noticeably weaker than in
165 the CHO cell experiments (Figure 1). This is due to the methodology used in each experiment. In the

166 transduction experiments (Figure 1), cells were incubated with virus at 37°C for three hours. For studies
167 evaluating the role of sialic acid and HSPGs, cells were pre-treated with enzyme for one hour at 37°C.
168 Then virus was then incubated with cells on ice for one hour following enzymatic digestion to prevent
169 repair and reconstitution of the cleaved heparin/sialic acid. This incubation on ice (and for a shorter
170 period of time) likely limits viral internalisation during the absorption step, seemingly more profoundly
171 for HAdV-C5/D49K than for the HAdV-C5.

172 Desmoglein 2 (DSG2) is the remaining well-established adenovirus receptor. It is described to interact
173 with species BII adenovirus, including HAdV-B3K, via low affinity, avidity dependent mechanism[33]. We
174 investigated whether HAdV-D49K might also interact with DSG2 by utilising surface plasmon resonance
175 (SPR), which we have previously used to establish a 66.9µM affinity between DSG2 and HAdV-D3K[34].
176 HAdV-D49K had no detectable affinity for DSG2 (Figure 3A), an unsurprising finding as DSG2 has never
177 been observed as a receptor for any adenovirus outside of species B.

178 HAdV-D49 fiber knob can interact with CAR, but does not require it for cell entry

179 We also used SPR to further probe the binding affinity of HAdV-D49K, and a mutant version, HAdV-
180 D49.KO1.K, for CD46 and CAR. This HAdV-D49.KO1.K mutant harbours the KO1 mutation previously
181 shown to ablate CAR binding in HAdV-C5K. The structure of the HAdV-D49.KO1.K fiber knob is presented
182 (see Supplemental Table 1 and Supplemental Figure 1)[35]. As precited, we did not observe binding
183 between either fiber knob protein and CD46. However, we were surprised to observe HAdV-D49K has a
184 detectable 0.19µM affinity for CAR which was ablated by the addition of the KO1 mutation (Figure 3A).

185 We next performed IC_{50} binding studies using recombinant HAdV-D49K protein on CHO-CAR and CHO-
186 BC1 cells and assessed the ability of the recombinant fiber knob protein to inhibit the binding of anti-
187 CAR or CD46 antibodies, respectively (Figure 3B). HAdV-D49K was able to block anti-CAR antibody
188 binding to CHO-CAR cells in a dose dependent manner (IC_{50} = 0.16µg/10^5 cells, Figure 3B). However, no

189 IC_{50} could be derived by using HAdV-D49K to block CD46 on CHO-BC1 cells, where HAdV-D49K was
190 unable to achieve more than 20% inhibition of antibody binding, suggesting weak or incidental CD46
191 interactions (Figure 3B). Therefore, these data support the findings from SPR and transduction
192 experiments that HAdV-D49K may engage CAR with low affinity, but does not engage CD46.

193 Our earlier findings indicated that HAdV-C5/D49K is not dependent upon CAR for cell entry (Figure 1),
194 however our *in vitro* biological inhibition and SPR assays demonstrate CAR binding affinity (Figure 3A, B).
195 We further investigated this finding by performing transduction blocking experiments of using the CAR
196 engaging HAdV-C5, and HAdV-C5/D49K with recombinant fiber knob protein of each virus in CHO-CAR
197 and CHO-K1 cells. As predicted, pre-incubation of CHO-CAR cells with recombinant HAdV-C5K efficiently
198 inhibited HAdV-C5 infection (Figure 3C), whilst blocking with HAdV-D49K inhibited infection by HAdV-C5
199 by approximately 50% (Figure 3D). Infecting CHO-CAR cells with HAdV-C5/D49K pseudotype and
200 attempting to block using HAdV-C5K (Figure 3E) or HAdV-D49K (Figure 3F) did not significantly inhibit
201 transduction efficiency. Finally, infection of CHO-K1 cells by HAdV-C5/D49K and blocking with HAdV-C5K
202 did not significantly inhibit transduction efficiency (Figure 3G), whilst blocking with HAdV-D49K reduced
203 transduction efficiency by approximately 50% (Figure 3H).

204 These data confirm that HAdV-D49K is capable of binding to CAR, at approximately 1000x lower affinity
205 than HAdV-C5[34], but in a manner able to inhibit HAdV-C5 binding. These data confirm HAdV-C5/D49K is
206 capable of entering cells though a non-CAR mediated pathway, since HAdV-C5K cannot inhibit HAdV-
207 C5/D49K transduction in CHO-CAR cells (Figure 3E). Interestingly, HAdV-C5/D49K was able to inhibit its
208 own viral infection only in the absence of CAR (Figure 3H).

209 One potential explanation for this activity is that the unknown alternative receptor to CAR has a lower
210 affinity for HAdV-D49K than CAR. Therefore, in the presence of CAR the recombinant fiber knob would
211 be sequestered on the higher affinity CAR receptor leaving the alternative receptor free to interact with

212 the virus. A very low affinity receptor would also likely depend upon avidity, so might not be observed
213 with single trimers of HAdV-D49K; a similar effect has previously been observed with HAdV-B3K and
214 DSG2[36]. This is supported by the observation what HAdV-D49K cannot transform cells as efficiently when
215 incubated on ice in the absence of CAR, while HAdV-C5 and HAdV-C5/B35K, which form high affinity
216 receptor interactions, are unencumbered (Figure 2).

217 HAdV-D49K may bind cells through a charge dependent mechanism

218 To investigate other closely related HAdV with homologous fiber-knob proteins we performed a BLASTp
219 search using the HAdV-D49K amino acid sequence. This search revealed that the HAdV-D30K protein is
220 highly homologous to HAdV-D49K, differing in just 4 amino acid residues (Figure 4A).

221 We solved the crystal structures of HAdV-D30K (Figure 4B, Supplementary Table 1, Supplementary
222 Figure 2) and HAdV-D49K (Figure 4C, Supplementary Table 1, Supplementary Figure 3) and demonstrate
223 that structurally, they are highly homologous (RMSD = 0.292$Å^2$). Residue 338 is not surface exposed on
224 either fiber knob protein and is likely to be functionally homologous (HAdV-D49 = Isoleucine338, HAdV-
225 D30 = Valine338). However, the remaining 3 residue differences, E339K, G331A, and Q332K (HAdV-D30K
226 → D49K) are surface exposed at the apex of each fiber knob monomer (Figure 4D, E). The E339K and
227 Q332K substitutions have opposing charges.

228 We investigated the relative transduction efficiency of HAdV-C5/D30K compared to HAdV-C5/D49K,
229 HAdV-C5, HAdV-C5.KO1, and HAdV-C5/D49.KO1.K in CHO-CAR (Figure 4F) and CHO-K1 cells (Figure 4G).
230 HAdV-C5 infected CHO-CAR cells efficiently whilst the CAR-binding ablated KO1 mutant version did not,
231 whilst HAdV-C5/49K and the corresponding mutant HAdV-C5/49KO1.K infected CHO-CAR cells with
232 similar efficiency as observed for HAdV-C5/D49K in Figure 1A. HAdV-C5/D30K infected CHO-CAR cells
233 with approximately 40% efficiency (Figure 4F). In CHO-K1 cells HAdV-C5/D49K and the KO1 mutant were
234 the only viruses which achieved efficient transduction. Surprisingly, given the high homology, to HAdV-

235 C5/D49K, the HAdV-C5/D30K pseudotype was inefficient in transducing CHO-K1 cells (<5% GFP^+, Figure
236 4G).

237 This profound difference in transduction efficiency between HAdV-C5/D30K and HAdV-C5/D49K must be
238 dependent upon the 3 surface exposed amino acid differences. We further investigated the effect of the
239 opposing charges at residue substitutions 339 and 332 (Figure 4A-E) by modelling the electrostatic
240 surface potential of the two fiber knob proteins, based on our crystal structures (Figure 5). The surface
241 potential maps reveal that whilst structural homology was high, they present radically different
242 electrostatic surface potential distributions. HAdV-D30K is significantly more acidic (pI = 5.57) than
243 HAdV-D49K (pI = 8.26) (Figure 5).

244 Thus, it seems probable that the interaction requires the basic electrostatic potential. This is
245 commensurate with the previous inference that its receptor is likely to be low affinity, as electrostatic
246 interfaces are often observed to be weaker than their ionic counterparts.

247 HAdV-C5/D49K is able to efficiently infect a large range of cancer cell lines

248 Given HAdV-C5/D49K infects cells independently of known adenovirus receptors we hypothesised that it
249 may form the basis of an efficient vector for cancer virotherapy applications. We therefore compared its
250 transduction efficiency to HAdV-C5 in panels of pancreatic (Figure 6), breast (Figure 7), and oesophageal,
251 colorectal, ovarian, and lung cancer cell lines (Figure 8).

252 In pancreatic cancer cell lines HAdV-C5/D49K was consistently more efficient at cellular transduction
253 than HAdV-C5. This improved activity ranged between 4.6x more efficient in MIA PaCa2 cells to 210.9x
254 more efficient in BxPc3 cells. The most effectively transduced cell line was Panc10 cells, producing $6x10^6$
255 RLU/mg of fluorescence, compared to the least efficient at just $4x10^5$ RLU/mg in Panc0403 cells. This
256 suggests that the large differences between HAdV-C5/D49K and HAdV-C5 transduction levels are likely
257 due to the variability in the expression of CAR (Figure 6). A similarly broad range of different relative

258 infection efficiencies were observed in the breast cancer cell lines studied. In MCF7 cells and BT20 cells
259 HAdV-C5/D49K was nearly 500 fold more efficient at transducing the cells due to these cells expressing
260 little CAR, with consequent poor levels of HAdV-C5 mediated transduction (Figure 7).

261 DLD-1 colorectal cancer cells were efficiently transduced by both HAdV-C5 and HAdV-C5/D49K vectors,
262 at $5x10^6$ and $6x10^6$ RLU/mg respectively. This is the only cell line where no significant difference in
263 infectivity was observed. A427 lung carcinoma cells are the only line where HAdV-C5 mediated cellular
264 transduction was more efficient than HAdV-C5/D49K (1.6x). Whilst HAdV-C5/D49K transduced A427 cell
265 very efficiently ($6x10^6$ RLU/mg) HAdV-C5 achieved unusually high transduction efficiency ($1x10^7$ RLU/mg)
266 (Figure 7). Therefore, this result is not due to inefficient HAdV-C5/D49K transduction, but unusually
267 efficient HAdV-C5 transduction.

268 Conclusions

269 Previous experiments using whole HAdV-D49 virus concluded that it utilises CD46 as its primary cellular
270 receptor[23]. The data described, generated using either purified HAdV-D49 fiber knob protein or a
271 pseudotyped HAdV-C5/D49K vector, demonstrate CD46 to be implausible as a receptor for HAdV-D49.

272 We demonstrate HAdV-D49 fiber knob has weak affinity for CAR, although it is not dependent upon this
273 interaction to mediate efficient cell entry, and in fact the presence of CAR may even inhibit cellular
274 transduction. In support of this we show a mutant vector, HAdV-C5/D49.KO1.K, containing mutations
275 within the fiber knob domain which ablate CAR affinity, was still able to efficiently transduce cells. Based
276 on the low efficiency by which HAdV-C5/D49K transduced cells when absorbed on ice and the
277 observation that HAdV-D49K is only capable of inhibiting HAdV-C5/D49K transduction in the absence of
278 CAR, we tentatively suggest that the unknown receptor is bound with weak affinity and may be avidity
279 dependent.

280 Regardless of the mechanism of interaction this study strongly suggests there is an as yet unknown
281 adenovirus receptor which mediates efficient transduction of a broad range of cell lines. This is
282 demonstrated by its ability to efficiently infect every cell line tested, throughout this study. The weakest
283 observed transduction was in Panc0403 cells where it achieved $4x10^5$ RLU/mg of luminescence. Whilst
284 this is not a particularly strong transduction efficiency, it is still significantly higher (33x, $P<0.05$) than
285 that of HAdV-C5. It is likely, therefore, that the HAdV-C5/D49K vector described here may be useful in
286 biotechnology applications to efficiently express proteins in difficult to transduce cell lines.

287 HAdV-C5/D49K represents a highly efficient gene transfer vehicle which is not restricted by any known
288 adenovirus tropism. It possesses a broad range of infectivity and has potential as both a laboratory
289 reagent, for the transient expression of transgenes, and as a therapeutic vaccine or oncolytic virus. For
290 oncolytic applications, it is likely that further refinement, such as the introduction of mutations known
291 to confer tumour selective replication, such as dl24 mutation[37–39] or the use of tumour specific
292 promoters such as hTERT[40] or survivin[41] to drive transgene therapeutic expression selectively within
293 tumour cells will be necessary to ensure tight tumour selectivity.

294 # Materials and Methods

295 **GFP transduction assay**

296 Adherent cells were seeded into a Nunc delta surface 96-well cell culture plate (ThermoFisher) at a
297 density of $5x10^4$ cells/well in 200µl of cell culture media and left to adhere overnight at 37˚C in a 5% CO_2
298 humidified atmosphere. Media was removed and cells washed twice with 200µl of PBS. Virus was added
299 at the desired concentration in 200µl of serum free RMPI 1640 and incubated under cell culture
300 conditions for 3hrs. The virus containing media was then removed and replaced with complete cell
301 culture media and the cells incubated for a further 45hrs. Cell culture media was then removed, the cells
302 washed twice with 200µl of PBS, trypsinised in 50µl of 0.05% Trypsin-EDTA (Gibco), and dissociated by
303 pipetting. The trypsinised cells were transferred to a 96-well V-bottom plate (ThermoFisher), neutralised
304 with 100µl of complete cell culture media, and pelleted by centrifugation at 1200RPM for 3mins.
305 Supernatant was removed, the cells washed once in 200µl of PBS, and resuspended in 100µl of 2% PFA
306 (PBS containing 2% w/v paraformaldehyde) and incubated at 4˚C for 15mins. Cells were again pelleted,
307 washed twice in 200µl PBS, then resuspended in 200µl PBS prior to analysis by flowcytometry.

308 Samples were analysed by flow cytometry on Attune NxT (ThermoFisher), voltages were set prior to
309 each experiment, for each cell type, using an uninfected cell population treated identically. Data was
310 analysed using FlowJo v10 (FlowJo, LLC), gating sequentially on singlets, cell population, and GFP
311 positive cells. Levels of infection were defined as the percentage of GFP positive cells (% +ve), and/or
312 Total Fluorescence (TF), defined as the percentage of GFP positive cells multiplied by the median
313 fluorescent intensity (MFI) of the GFP positive population. These measures are distinct in that % +ve
314 describes the total proportion of cells infected, and TF describes the total efficiency of transgene
315 delivery.

316 **Luciferase transduction assay**

317 Luciferase infectivity assays were performed using the luciferase assay system kit (Promega). Cells were
318 seeded into a Nunc delta surface 96-well cell culture plate (ThermoFisher) at a density of $2x10^4$
319 cells/well in 200µl of cell culture media and left to adhere overnight at 37˚C in a 5% CO_2 humidified
320 atmosphere. Media was removed and cells washed once with 200µl of PBS. Luciferase transgene
321 encoding replication incompetent viruses were added to the necessary wells at the required titre in
322 200µl of serum free RMPI 1640 and incubated under cell culture conditions for 3hrs. The virus
323 containing media was then removed and replaced with complete cell culture media and the cells
324 incubated for a further 45hrs. Cell culture media was then removed, the cells washed twice with 200µl
325 of PBS, and were then lysed in 100µl of cell culture lysis buffer (part of the Promega kit) diluted to 1x in
326 ddH_2O. The plate was then frozen at -80˚C.

327 After thaw, 10µl of lysate from the cell culture plate mixed then was transferred to a white Nunc 96-
328 microwell plate (ThermoFisher) and 100µl of luciferase assay reagent (Promega Kit) added. Luciferase
329 activity was then measured in relative light units (RLU) by plate reader (Clariostar, BMG Labtech). Total
330 protein concentration was determined in the lysate using the Pierce BCA protein assay kit
331 (Thermofisher) according to the manufacturers protocol, absorbance was measured on an iMark
332 microplate absorbance reader (BioRad).

333 Relative virus infection was determined by normalising the measured luciferase intensity to the total
334 protein concentration (RLU was divided by protein concentration). This gave a final infectivity readout in
335 RLU/mg of protein.

336 **Blocking of virus infection with recombinant fiber knob protein**

337 This assay was also performed using the luciferase assay system kit (Promega). Cells were seeded into a
338 Nunc delta surface 96-well cell culture plate (ThermoFisher) at a density of $20x10^3$ cells/well in 200µl of

339 cell culture media and left to adhere overnight at 37˚C in a 5% CO_2 humidified atmosphere. Media was
340 removed and cells washed 2x with 200µl of cold PBS and the plate cooled on ice. 20pg/cell of
341 recombinant adenovirus fiber knob was added to each well in 200µl of cold PBS and incubated on ice in
342 a 4˚C cold room for 1hr. Media was then removed and luciferase transgene encoding replication
343 incompetent viruses added to the necessary wells at the required titre in 200µl of cold serum free RMPI
344 1640 and incubated on ice in a 4˚C cold room for 1hr. The virus containing media was then removed and
345 replaced with complete cell culture media and the cells incubated for a further 45hrs under normal cell
346 culture conditions. From this point forward the assay is identical to the GFP and luciferase transduction
347 assays.

348 **Heparinase and Neuraminidase transduction assays**

349 Cells were seeded at a density of $5x10^4$ cells/well in a flat bottomed 96 well cell culture plate and
350 incubated overnight at 37°C to adhere. Cells were washed twice with 200µl of PBS. 50µl of
351 neuraminidase (from Vibrio Cholera, Merk) at a concentration of 50mU/ml, or 50µl of Heparinase III
352 (from Flavobacterium heparinum, Merck) at a concentration of 1U/ml was diluted in serum free media,
353 added to the appropriate wells, and incubated for 1hr at 37°C. Cells were cooled on ice and washed
354 twice with 200µl of PBS. Green Fluorescent Protein (GFP) expressing, replication incompetent viruses
355 were added to the appropriate wells at a concentration of 5000 viral particles per cell, in 100µl of serum
356 free media, at 4°C, and incubated on ice for 1hr. Serum free media alone was added to uninfected
357 control wells. Cells were washed twice with 200µl of cold PBS, complete media added (DMEM, 10% FCS)
358 and incubated for 48hrs at 37°C. Cells were then trypsinised and transferred to a 96 well V-bottom plate,
359 washed twice in 200µl of PBS and fixed in 2% paraformaldehyde containing PBS for 20mins before wash,
360 and resuspension in 200µl of PBS.

361 Samples were analysed by flow cytometry on Attune NxT (ThermoFisher), voltages were set prior to
362 each experiment, for each cell type, using an uninfected cell population treated identically. Data was
363 analysed using FlowJo v10 (FlowJo, LLC), gating sequentially on singlets, cell population, and GFP
364 positive cells. Levels of infection were defined as the percentage of GFP positive cells (% +ve), and/or
365 Total Fluorescence (TF), defined as the percentage of GFP positive cells multiplied by the median
366 fluorescent intensity (MFI) of the GFP positive population. These measures are distinct in that % +ve
367 describes the total proportion of cells infected, and TF describes the total efficiency of transgene
368 delivery.

369 **Surface Plasmon Resonance**

370 Surface plasmon resonance was performed, in triplicate, as previously described, using recombinant
371 HAdV-D49K protein[34]. Approximately 5000 RU of Recombinant Human Desmoglein-2 Fc Chimera Protein
372 (R&D Systems, Catalogue number 947-DM-100) was amine coupled to a CM5 sensor chip at a slow flow-
373 rate of 10 µl/min to ensure uniform distribution on the chip surface.

374 **Competition Inhibition Assay**

375 Competition inhibition assays of antibody binding to cell surface receptors were performed as previously
376 described[34].

377 **Generation of recombinant fiber knob proteins**

378 Recombinant fiber knob proteins used in transduction inhibition, antibody blocking, and crystallisation
379 experiments were produced as previous described[24,34]. Briefly, pQE-30 vectors containing the sequence
380 of the relevant fiber knob protein, spanning from 13 amino acids preceeding the TLW motif to the stop
381 codon, were transformed into SG13009 E.coli harbouring the pREP-4 plasmid. 1L of these E.coli were
382 grown to OD0.6 and protein expression induced with a final concentration of 0.5mM IPTG. E.coli were

383 harvested by centrifugation and resuspended in 50ml lysis buffer (50 mM Tris, pH 8.0, 300 mM NaCl, 1%
384 (v/v) NP40, 1 mg/ml Lysozyme, 1 mM β-mercaptoethanol). Sample was then loaded onto a HisTrap FF
385 Crude column and eluted by imidazole. Fractions determined to contain protein of interest were then
386 concentrated to <1ml total volume and purified by size exclusion chromatography using a Superdex 200
387 10/300 GL Increase column.

388 Fiber knob protein crystallisation and structure determination by X-Ray 389 crystallography

390 HAdV-D49K, HAdV-D49.KO1.K, and HAdV-D30K were crystallised in the same manner as previously
391 described[24,34]. Both HAdV-D49K and HAdV-D49.KO1.K crystals formed in 0.1M MMT, 25% w/v PEG1500,
392 whilst HAdV-D30K crystallised in 0.1M SPG, 25% w/v PEG 1500. All crystals formed in 2-7 days. Data
393 collection statistics, PDB deposition numbers, sample map density images, and validation statistics are
394 described in supplementary table 1 and supplementary figures 1-3.

395 Calculation of electrostatic surface potentials and pIs

396 Electrostatic surface potential and isoelectric points were calculated at pH 7.2 using the PDB2PQR Server
397 (V 2.1.1)[42] as previous described[24].

398 RMSD calculation, sequence alignment, and imaging of crystal structures

399 Alignments were performed using the Clustal Omega multiple sequence alignment algorithm and
400 visualised with BioEdit[43,44]. RMSD calculations were performed using the 'align' command in PyMOL 2.0,
401 which was also used to visualise protein structures[45].

402 **Acknowledgements**

403 ATB was funded by a Tenovus Cancer Care PhD studentship (reference PhD2015/L13). GM was
404 supported by a Cancer Research UK ECMC centre award (C7838/A25173). JAD is funded by a Cancer
405 Research UK Biotherapeutic Programme award (reference C52915/A29104). EM is supported by a
406 Wellcome Trust ISSF Translational Kickstarter Award (reference 517732). RMM was supported by the
407 Cardiff University Research Opportunities Placement (CUROP). PJR and ALP are funded by HEFCW. The
408 authors acknowledge the Diamond Light Source for beamtime (proposal MX18812) and the staff of
409 beamline I03 for assistance with diffraction data collection. The authors acknowledge Johanne Pentier
410 for technical assistance with SPR data collection, as well as Aaron Wall and Anna Fuller for assistance
411 with FPLC.

412 # References

413 1. Baker, A. T., Aguirre-Hernández, C., Halldén, G. & Parker, A. L. Designer Oncolytic Adenovirus:
414 Coming of Age. *Cancers* **10**, 201 (2018).
415 2. Russell, W. C. Adenoviruses: update on structure and function. *J. Gen. Virol.* **90**, 1–20 (2009).
416 3. Stanton, R. J., McSharry, B. P., Armstrong, M., Tomasec, P. & Wilkinson, G. W. G. Re-engineering
417 adenovirus vector systems to enable high-throughput analyses of gene function. *BioTechniques* **45**,
418 659–662, 664–668 (2008).
419 4. Alba, R., Baker, AndrewH. & Nicklin, StuartA. Vector Systems for Prenatal Gene Therapy: Principles
420 of Adenovirus Design and Production. in *Prenatal Gene Therapy* (eds. Coutelle, C. & Waddington, S.
421 N.) 55–84 (Humana Press, 2012). doi:10.1007/978-1-61779-873-3_4.
422 5. Weaver, E. A. & Barry, M. A. Low Seroprevalent Species D Adenovirus Vectors as Influenza Vaccines.
423 *PLOS ONE* **8**, e73313 (2013).
424 6. Atasheva, S., Yao, J. & Shayakhmetov, D. M. Innate immunity to adenovirus: lessons from mice. *FEBS*
425 *Lett.* **593**, 3461–3483 (2019).
426 7. Ahi, Y. S., Bangari, D. S. & Mittal, S. K. Adenoviral Vector Immunity: Its Implications and
427 circumvention strategies. *Curr. Gene Ther.* **11**, 307–320 (2011).
428 8. Dakin, R. S., Parker, A. L., Delles, C., Nicklin, S. A. & Baker, A. H. Efficient transduction of primary
429 vascular cells by the rare adenovirus serotype 49 vector. *Hum. Gene Ther.* **26**, 312–319 (2015).
430 9. Abbink, P. *et al.* Comparative Seroprevalence and Immunogenicity of Six Rare Serotype
431 Recombinant Adenovirus Vaccine Vectors from Subgroups B and D. *J. Virol.* **81**, 4654–4663 (2007).
432 10. Zhao, H. *et al.* Seroprevalence of Neutralizing Antibodies against Human Adenovirus Type-5 and
433 Chimpanzee Adenovirus Type-68 in Cancer Patients. *Front. Immunol.* **9**, (2018).

434 11. Teigler, J. E., Iampietro, M. J. & Barouch, D. H. Vaccination with Adenovirus Serotypes 35, 26, and 48
435 Elicits Higher Levels of Innate Cytokine Responses than Adenovirus Serotype 5 in Rhesus Monkeys. *J.*
436 *Virol.* **86**, 9590–9598 (2012).
437 12. Dyer, A. *et al.* Oncolytic Group B Adenovirus Enadenotucirev Mediates Non-apoptotic Cell Death
438 with Membrane Disruption and Release of Inflammatory Mediators. *Mol Ther Oncolytics* **4**, 18–30
439 (2017).
440 13. Di, Y., Seymour, L. & Fisher, K. Activity of a group B oncolytic adenovirus (ColoAd1) in whole human
441 blood. *Gene Ther.* **21**, 440–443 (2014).
442 14. Human adenovirus B strain ColoAd1, complete genome. (2009).
443 15. Long-term Safety Follow-up of Participants Exposed to the Candidate Ebola Vaccines Ad26.ZEBOV
444 and/or MVA-BN-Filo - Full Text View - ClinicalTrials.gov.
445 https://clinicaltrials.gov/ct2/show/NCT02661464?term=adenovirus&recrs=a&cond=ebola&rank=1.
446 16. A Study to Assess Ebola Vaccines ChAd3-EBO-Z and Ad26.ZEBOV - Full Text View - ClinicalTrials.gov.
447 https://clinicaltrials.gov/ct2/show/NCT02495246?term=ad26&draw=1&rank=2.
448 17. Vogels, R. *et al.* Replication-Deficient Human Adenovirus Type 35 Vectors for Gene Transfer and
449 Vaccination: Efficient Human Cell Infection and Bypass of Preexisting Adenovirus Immunity. *J. Virol.*
450 **77**, 8263–8271 (2003).
451 18. Schnurr, D. & Dondero, M. E. Two New Candidate Adenovirus Serotypes. *Intervirology* **36**, 79–83
452 (1993).
453 19. De Jong, J. C. *et al.* Adenoviruses from Human Immunodeficiency Virus-Infected Individuals,
454 Including Two Strains That Represent New Candidate Serotypes Ad50 and Ad51 of Species B1 and
455 D, Respectively. *J. Clin. Microbiol.* **37**, 3940–3945 (1999).
456 20. Ishiko, H. *et al.* Novel Human Adenovirus Causing Nosocomial Epidemic Keratoconjunctivitis. *J. Clin.*
457 *Microbiol.* **46**, 2002–2008 (2008).

458 21. Human adenovirus 49 gene for fiber protein, partial cds, strain: T87-677. (2016).
459 22. Al Qurashi, Y. M. A., Alkhalaf, M. A., Lim, L., Guiver, M. & Cooper, R. J. Sequencing and phylogenetic
460 analysis of the hexon, fiber, and penton regions of adenoviruses isolated from AIDS patients. *J. Med.*
461 *Virol.* **84**, 1157–1165 (2012).
462 23. Lemckert, A. A. C. *et al.* Generation of a novel replication-incompetent adenoviral vector derived
463 from human adenovirus type 49: manufacture on PER.C6 cells, tropism and immunogenicity. *J. Gen.*
464 *Virol.* **87**, 2891–2899 (2006).
465 24. Baker, A. T., Mundy, R. M., Davies, J. A., Rizkallah, P. J. & Parker, A. L. Human adenovirus type 26
466 uses sialic acid–bearing glycans as a primary cell entry receptor. *Sci. Adv.* **5**, eaax3567 (2019).
467 25. Gaggar, A., Shayakhmetov, D. M. & Lieber, A. CD46 is a cellular receptor for group B adenoviruses.
468 *Nat. Med.* **9**, 1408–1412 (2003).
469 26. Roelvink, P. W. *et al.* The Coxsackievirus-Adenovirus Receptor Protein Can Function as a Cellular
470 Attachment Protein for Adenovirus Serotypes from Subgroups A, C, D, E, and F. *J. Virol.* **72**, 7909–
471 7915 (1998).
472 27. Alba, R. *et al.* Coagulation factor X mediates adenovirus type 5 liver gene transfer in non-human
473 primates (*Microcebus murinus*). *Gene Ther.* **19**, 109–113 (2012).
474 28. Alba, R. *et al.* Identification of coagulation factor (F)X binding sites on the adenovirus serotype 5
475 hexon: effect of mutagenesis on FX interactions and gene transfer. *Blood* **114**, 965–971 (2009).
476 29. Parker, A. L. *et al.* Multiple vitamin K-dependent coagulation zymogens promote adenovirus-
477 mediated gene delivery to hepatocytes. *Blood* **108**, 2554–2561 (2006).
478 30. Waddington, S. N. *et al.* Adenovirus Serotype 5 Hexon Mediates Liver Gene Transfer. *Cell* **132**, 397–
479 409 (2008).
480 31. Burmeister, W. P., Guilligay, D., Cusack, S., Wadell, G. & Arnberg, N. Crystal Structure of Species D
481 Adenovirus Fiber Knobs and Their Sialic Acid Binding Sites. *J. Virol.* **78**, 7727–7736 (2004).

482 32. Arnberg, N., Edlund, K., Kidd, A. H. & Wadell, G. Adenovirus Type 37 Uses Sialic Acid as a Cellular
483 Receptor. *J. Virol.* **74**, 42–48 (2000).
484 33. Vassal-Stermann, E. *et al.* CryoEM structure of adenovirus type 3 fibre with desmoglein 2 shows an
485 unusual mode of receptor engagement. *Nat. Commun.* **10**, 1181 (2019).
486 34. Baker, A. T. *et al.* Diversity within the adenovirus fiber knob hypervariable loops influences primary
487 receptor interactions. *Nat. Commun.* **10**, 741 (2019).
488 35. Jakubczak, J. L. *et al.* Adenovirus Type 5 Viral Particles Pseudotyped with Mutagenized Fiber Proteins
489 Show Diminished Infectivity of Coxsackie B-Adenovirus Receptor-Bearing Cells. *J. Virol.* **75**, 2972–
490 2981 (2001).
491 36. Vassal-Stermann, E. *et al.* Mapping of Adenovirus of serotype 3 fibre interaction to desmoglein 2
492 revealed a novel 'non-classical' mechanism of viral receptor engagement. *Sci. Rep.* **8**, (2018).
493 37. Uusi-Kerttula, H. *et al.* Ad5NULL-A20 - a tropism-modified, αvβ6 integrin-selective oncolytic
494 adenovirus for epithelial ovarian cancer therapies. *Clin. Cancer Res.* clincanres.1089.2018 (2018)
495 doi:10.1158/1078-0432.CCR-18-1089.
496 38. Loskog, A. *et al.* Immunostimulatory AdCD40L gene therapy combined with low-dose
497 cyclophosphamide in metastatic melanoma patients. *Br J Cancer* **114**, 872–80 (2016).
498 39. Man, Y. K. S. *et al.* The Novel Oncolytic Adenoviral Mutant Ad5-3Δ-A20T Retargeted to αvβ6
499 Integrins Efficiently Eliminates Pancreatic Cancer Cells. *Mol. Cancer Ther.* **17**, 575–587 (2018).
500 40. Onimaru, M. *et al.* Combination with low-dose gemcitabine and hTERT-promoter-dependent
501 conditionally replicative adenovirus enhances cytotoxicity through their crosstalk mechanisms in
502 pancreatic cancer. *Cancer Lett* **294**, 178–86 (2010).
503 41. Wang, W. *et al.* Survivin promoter-regulated oncolytic adenovirus with Hsp70 gene exerts effective
504 antitumor efficacy in gastric cancer immunotherapy. *Oncotarget* **5**, 150–160 (2013).

42. Jurrus, E. *et al.* Improvements to the APBS biomolecular solvation software suite. *Protein Sci. Publ. Protein Soc.* **27**, 112–128 (2018).

43. Sievers, F. *et al.* Fast, scalable generation of high-quality protein multiple sequence alignments using Clustal Omega. *Mol. Syst. Biol.* **7**, 539–539 (2011).

44. Li, W. *et al.* The EMBL-EBI bioinformatics web and programmatic tools framework. *Nucleic Acids Res.* **43**, W580-4 (2015).

45. Schrödinger, LLC. The PyMOL Molecular Graphics System, Version 2.0.

514 **Figure Legends:**

515 **Figure 1: HAdV-C5/D49K infection is not dependent upon CAR or CD46.** GFP transduction assays show
516 that both HAdV-C5 and HAdV-C5/D49K is capable of efficiently transducing CHO-CAR cells, Chinese
517 Hamster Ovary cells expressing human CAR (A). CHO-BC1 cells, expressing human CD46 isoform BC1, are
518 efficiently transduced by both HAdV-C5/B35K and HAdV-C5/D49K (B). CHO-K1 cells, which do not
519 express any known adenovirus fiber-knob receptors are not efficiently transduced by HAdV-C5 or HAdV-
520 C5/B35K, but is efficiently transduced by HAdV-C5/D49K (C).

521 **Figure 2: HAdV-C5/49K transduction is not dependent upon HSPGs, sialic acid bearing glycans or**
522 **Desmoglein 2 (DSG2).** Treatment of CHO-K1 (A) or SKOV-3 (B) cells with heparinase diminishes the
523 infectivity of HAdV-C5 via the FX dependent pathway, but HAdV-C5/D49K transduction efficiency is
524 unaffected by heparinase treatment. Cleavage of cell surface sialic acid has no effect upon the
525 transduction efficiency of any of the tested viruses in CHO-K1 cells (C), however, in SKOV-3 cells both
526 HAdV-C5/B35K and HAdV-C5/D49K efficiency increases following neuraminidase treatment (D). Cells
527 were infected with 5,000 viral particles per cell of replication deficient HAdV-C5, HAdV-C5/B35K, or
528 HAdV-C5/49K expressing a GFP transgene, n=3 error is ±SD. *= $P<0.05$, **= $P<0.01$, ***= $P<0.005$, ,
529 ****= $P<0.001$.

530 **Figure 3: HAdV-D49K interacts with CAR but is not dependent upon it as an entry receptor.** Surface
531 plasmon resonance experiments show that HAdV-D49K is capable of binding to CAR with a KD of
532 0.19µM, however the HAdV-D49.KO1.K mutant cannot bind to CAR and neither protein forms a
533 measurable interaction with DSG2 or CD46 (A). Antibody binding inhibition assays show that HAdV-D49K
534 blocks anti-CAR antibody binding to CHO-CAR cells with an IC50 value of 0.16µg/10^5 cells but is unable to
535 inhibit abti-CD46 antibody binding to CHO-BC1 cells by more than 25% (B). Preincubation of CHO-CAR
536 cells with HAdV-C5K inhibits HAdV-C5 infection (C), preincubation with HAdV-D49K also inhibits HAdV-

537 C5 infection by approximately 50% (D). Conversely HAdV-C5/D49K transduction was uninhibited in by
538 either HAdV-C5K (E) or HAdV-D49K (F) in CHO-CAR cells. In CHO-K1 cells there was no significant
539 decrease in HAdV-C5/D49K transduction efficiency when blockaded by HAdV-C5K (G), but an
540 approximately 50% decrease in transduction was observed in CHO-K1 cells following blockade with
541 HAdV-D49K (H). Cells were infected with 5,000 viral particles per cell of replication deficient HAdV-C5 or
542 HAdV-C5/D49K expressing a luciferase transgene, with and without blockade by 20µg of recombinant
543 HAdV-C5 or HAdV-D49 fiber knob protein. n=3 error is ±SD. *= P<0.05, **= P<0.01, ***= P<0.005, ****=
544 P<0.001.

545 **Figure 4: HAdV-D49K differs from HAdV-D30K in only three surface exposed amino acids but is**
546 **dependent upon CAR to infect CHO cells.** ClustalΩ sequence alignment (numbering based on whole
547 fiber sequence) of HAdV-D30K and HAdV-D49K reveals four amino acid differences (A). Viewed from the
548 apex down the three fold axis, as if towards the viral capsid, the crystal structures of HAdV-D30K (B) and
549 HAdV-D49K reveal that three of these residues are surface exposed. These residues can be seen
550 projecting into the solvent from loops on the apex of HAdV-D30K (D) and HAdV-D49K (E), residue
551 numbers and names correspond to the fiber-knob protein depicted in that frame. Sticks representing
552 residues belonging to HAdV-D30K and HAdV-D49K are seen in pink and green, respectively. Transduction
553 assays demonstrate that HAdV-C5/D30K is capable of infecting CHO-CAR cells with moderate efficiency
554 (F) it is not capable of infecting CHO-K1 cells (G), whilst the HAdV-C5/D49.KO1.K mutant is capable of
555 infecting both cell lines. Cells were infected with 5,000 viral particles per cell of replication deficient
556 HAdV-C5 or HAdV-C5/D49K expressing a luciferase transgene, with and without blockade by 20µg of
557 recombinant HAdV-C5 or HAdV-D49 fiber knob protein.

558 **Figure 5: The differences in residues between HAdV-D30K and HAdV-D49K have a large effect on the**
559 **surface electrostatic potential of the fiber knob.** The calculated pI of HAdV-D30K and HAdV-D49K is
560 very different as a result of the residue changes, which are shown as green sticks as they occur in that

561 fiber knob protein. The calculated electrostatic surface potential at pH7.35 is projected on a -10mV to
562 +10mV ramp (Red to Blue). HAdV-D49K can be seen to have much more basic potential around the apex
563 where the residue substitutions are.

564 **Figure 6: HAdV-C5/D49K transduces human pancreatic cancer cell lines with high efficiency**.
565 Transduction efficiency was assessed using HAdV-C5/D49K (shown as Ad5/49k in the figure) and HAdV-
566 C5 (shown as Ad5 in the figure) in all tested pancreatic cancer cell lines (names given above plots). Cells
567 were infected with 5,000 viral particles per cell of replication deficient HAdV-C5 or HAdV-C5/49K
568 expressing a luciferase transgene, n=3. *= P<0.05, **= P<0.01, ***= P<0.005, ****= P<0.001

569 **Figure 7: HAdV-C5/D49K transduces human breast cancer cell lines with high efficiency.** Transduction
570 efficiency was assessed using HAdV-C5/D49K (shown as Ad5/49k in the figure) and HAdV-C5 (shown as
571 Ad5 in the figure) in all tested pancreatic cancer cell lines (names given above plots). Cells were infected
572 with 5,000 viral particles per cell of replication deficient HAdV-C5 or HAdV-C5/49K expressing a
573 luciferase transgene, n=3. *= P<0.05, **= P<0.01, ***= P<0.005, ****= P<0.001

574 **Figure 8: HAdV-C5/D49K can transduce human lung, oesophageal, colorectal, and ovarian cancer cell**
575 **lines with high efficiency.** Transduction efficiency was assessed using HAdV-C5/D49K (shown as
576 Ad5/49k in the figure) and HAdV-C5 (shown as Ad5 in the figure) in all tested cancer cell lines (names
577 given above plots). NCI-H460, A427, and A549 cells are lung cancer cell lines, Kyse-30, DLD-1, and SKOV-
578 3 cells are oesophageal, colorectal, and ovarian cancer cell lines, respectively (names given above plots).
579 Cells were infected with 5,000 viral particles per cell of replication deficient HAdV-C5 or HAdV-C5/49K
580 expressing a luciferase transgene, n=3 error is ±SD. *= P<0.05, **= P<0.01, ***= P<0.005, ****= P<0.001

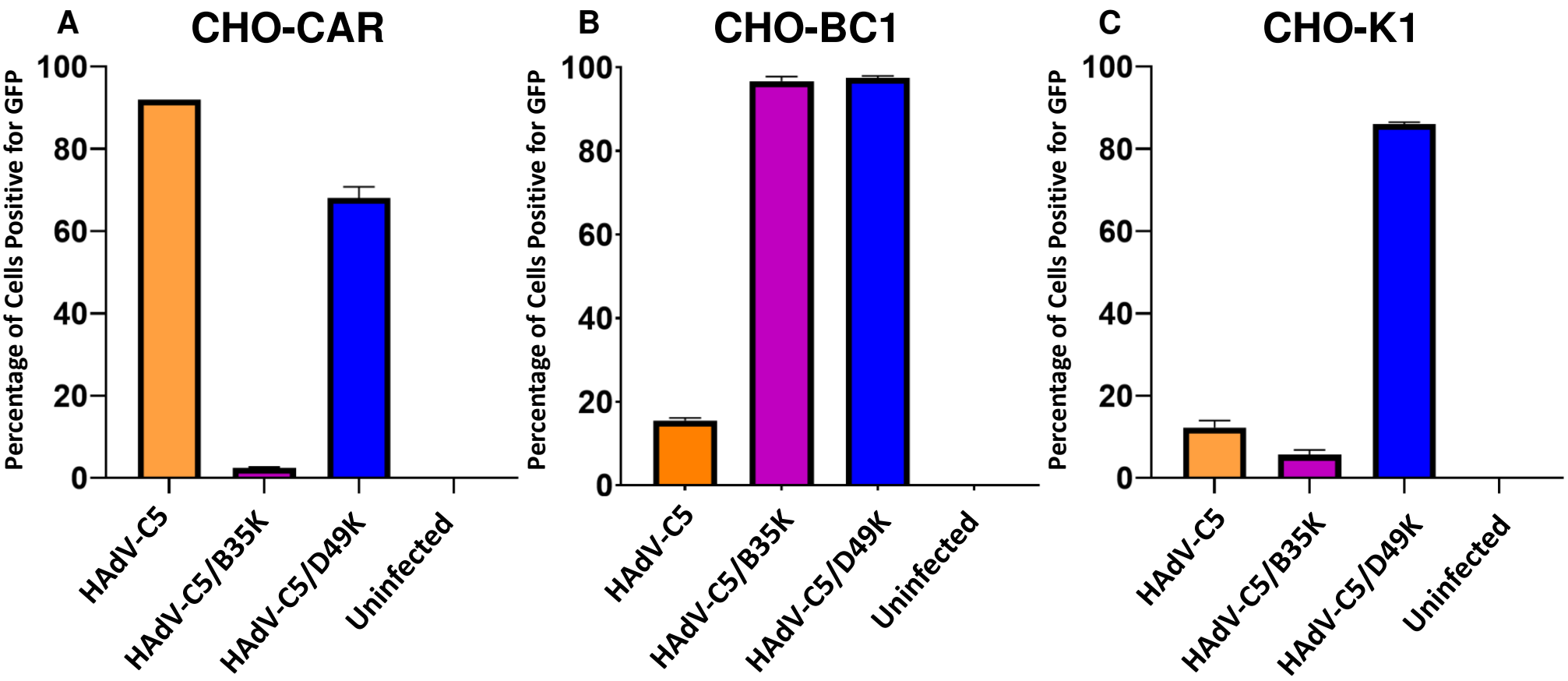
A
CHO-CAR
B
CHO-BC1
C
CHO-K1
Percentage of Cells Positive for GFP
100
80
60
40
20
0
HAdV-C5
HAdV-C5/B35K
HAdV-C5/D49K
Uninfected

Figure 1

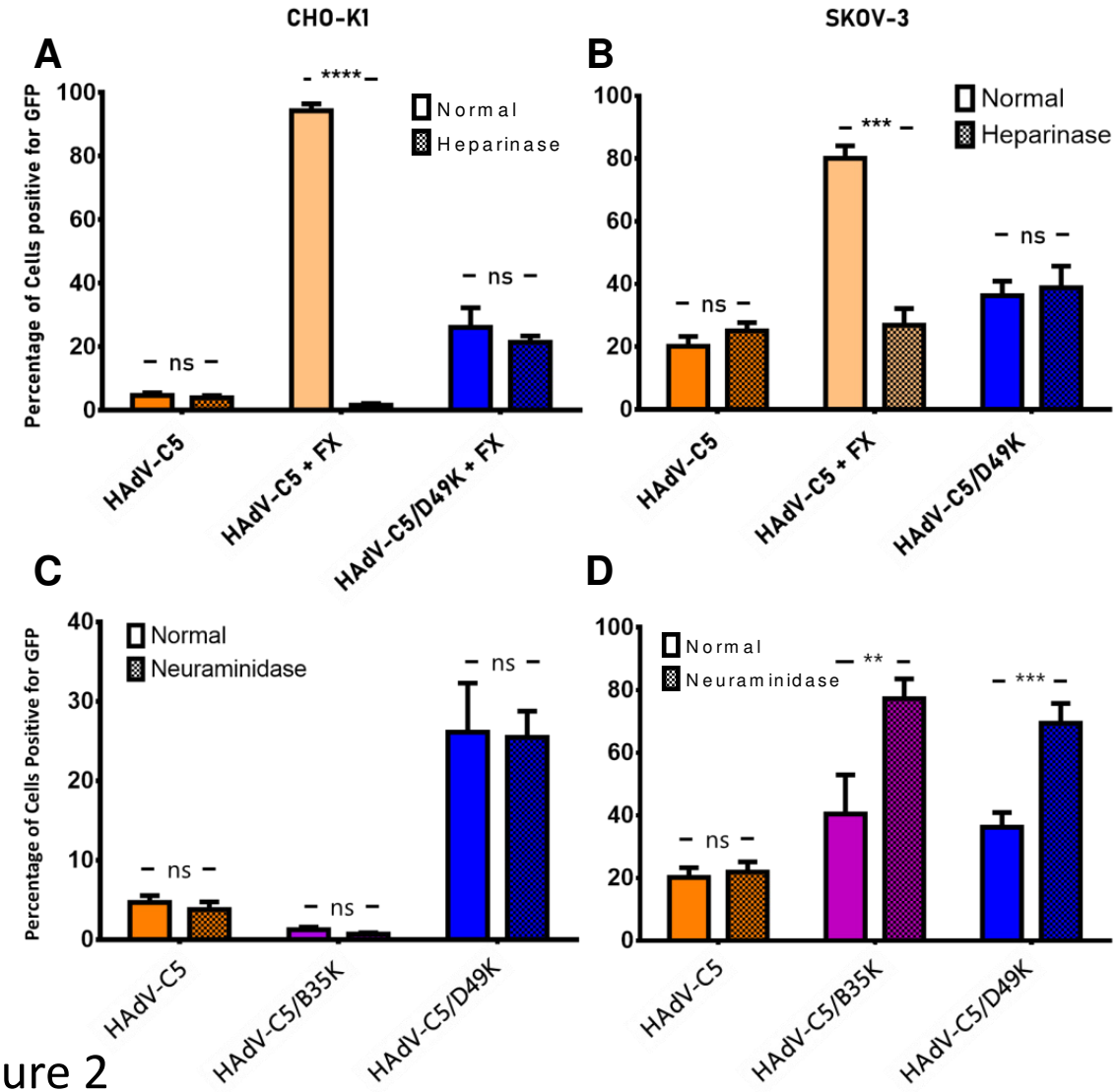
CHO-K1
SKOV-3
A
B
C
D
Percentage of Cells positive for GFP
Percentage of Cells Positive for GFP
Normal
Heparinase
Neuraminidase
ns
****
***
**
HAdV-C5
HAdV-C5 + FX
HAdV-C5/D49K + FX
HAdV-C5/D49K
HAdV-C5/B35K

Figure 2

A

	HAdV-D49K			HAdV-D49.K01.K		
	K_{on} (M^{-1} s^{-1})	K_{off} (s^{-1})	K_D (μM)	K_{on} (M^{-1} s^{-1})	K_{off} (s^{-1})	K_D (μM)
CAR	6.1×10^3	0.0012	0.19	nb	nb	No binding
CD46	nb	nb	No binding	nb	nb	No binding
DSG2	nb	nb	No binding	nb	nb	No binding

nm = kinetics too fast to measure
nb = no binding

B

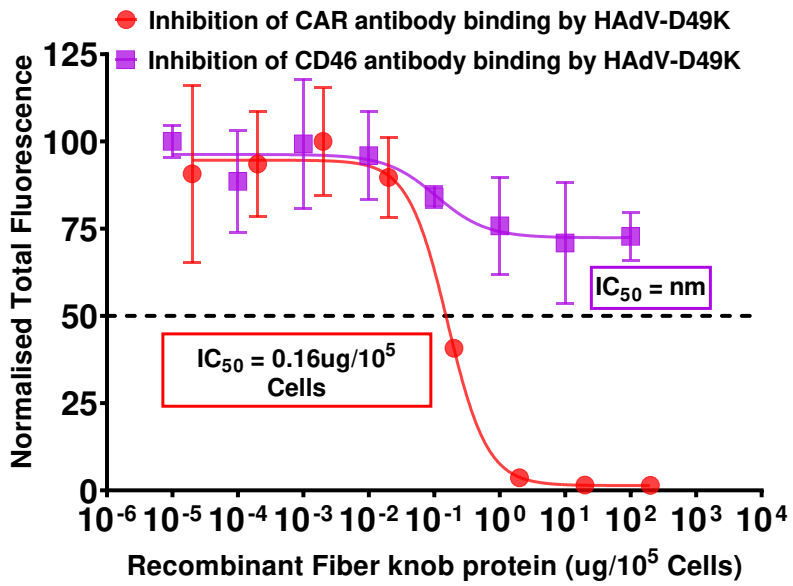

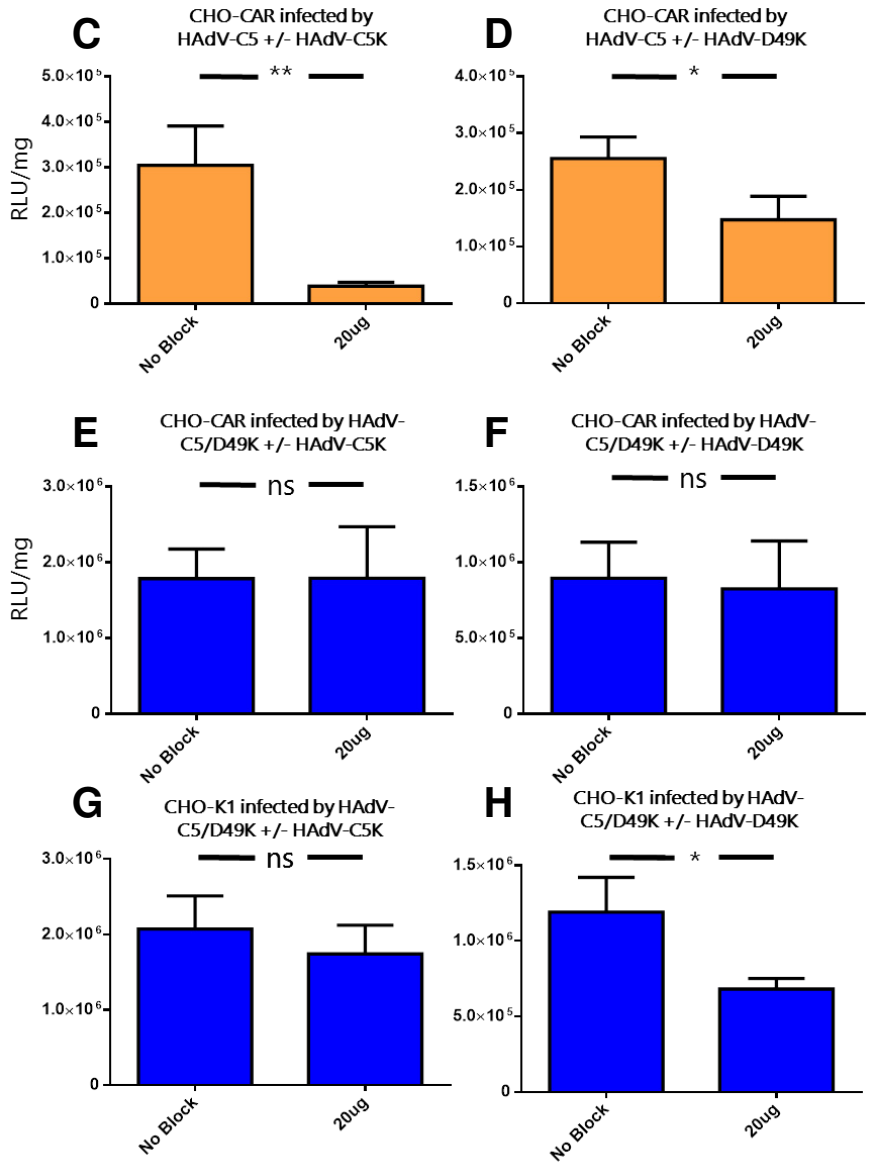

Figure 3

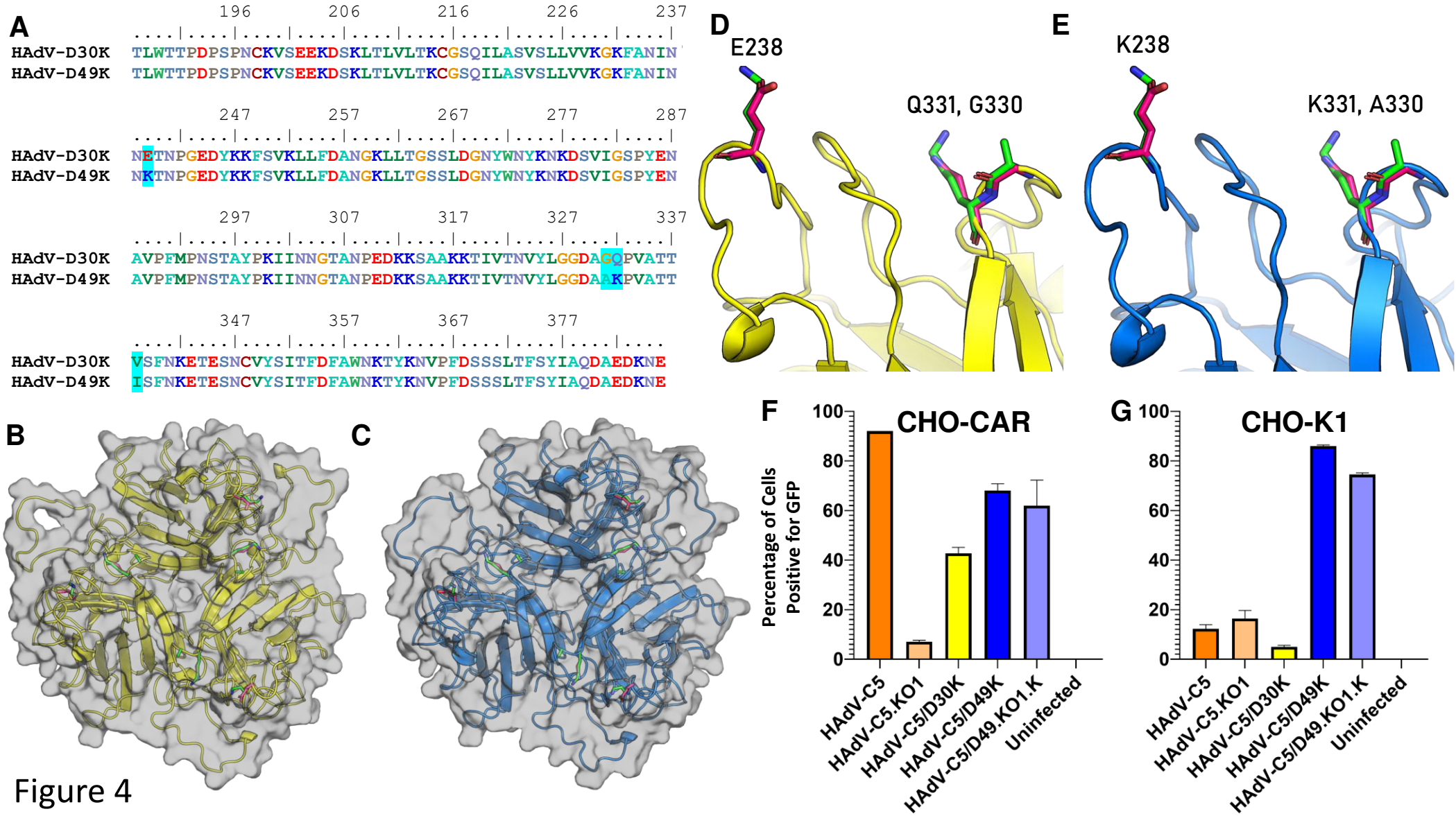
A
196 206 216 226 237
HAdV-D30K TLWTTPDPSPNCKVSEEKDSKLTLVLTKCGSQILASVSLLVVKGKFANIN
HAdV-D49K TLWTTPDPSPNCKVSEEKDSKLTLVLTKCGSQILASVSLLVVKGKFANIN
247 257 267 277 287
HAdV-D30K NETNPGEDYKKFSVKLLFDANGKLLTGSSLDGNYWNYKNKDSVIGSPYEN
HAdV-D49K NKTNPGEDYKKFSVKLLFDANGKLLTGSSLDGNYWNYKNKDSVIGSPYEN
297 307 317 327 337
HAdV-D30K AVPFMPNSTAYPKIINNGTANPEDKKSAAKKTIVTNVYLGGDAGQPVATT
HAdV-D49K AVPFMPNSTAYPKIINNGTANPEDKKSAAKKTIVTNVYLGGDAAKPVATT
347 357 367 377
HAdV-D30K VSFNKETESNCVYSITFDFAWNKTYKNVPFDSSSLTFSYIAQDAEDKNE
HAdV-D49K ISFNKETESNCVYSITFDFAWNKTYKNVPFDSSSLTFSYIAQDAEDKNE
B
C
D
E238
Q331, G330
E
K238
K331, A330
F
CHO-CAR
Percentage of Cells Positive for GFP
100
80
60
40
20
0
HAdV-C5
HAdV-C5.KO1
HAdV-C5/D30K
HAdV-C5/D49K
HAdV-C5/D49.KO1.K
Uninfected
G
CHO-K1
100
80
60
40
20
0
HAdV-C5
HAdV-C5.KO1
HAdV-C5/D30K
HAdV-C5/D49K
HAdV-C5/D49.KO1.K
Uninfected

Figure 4

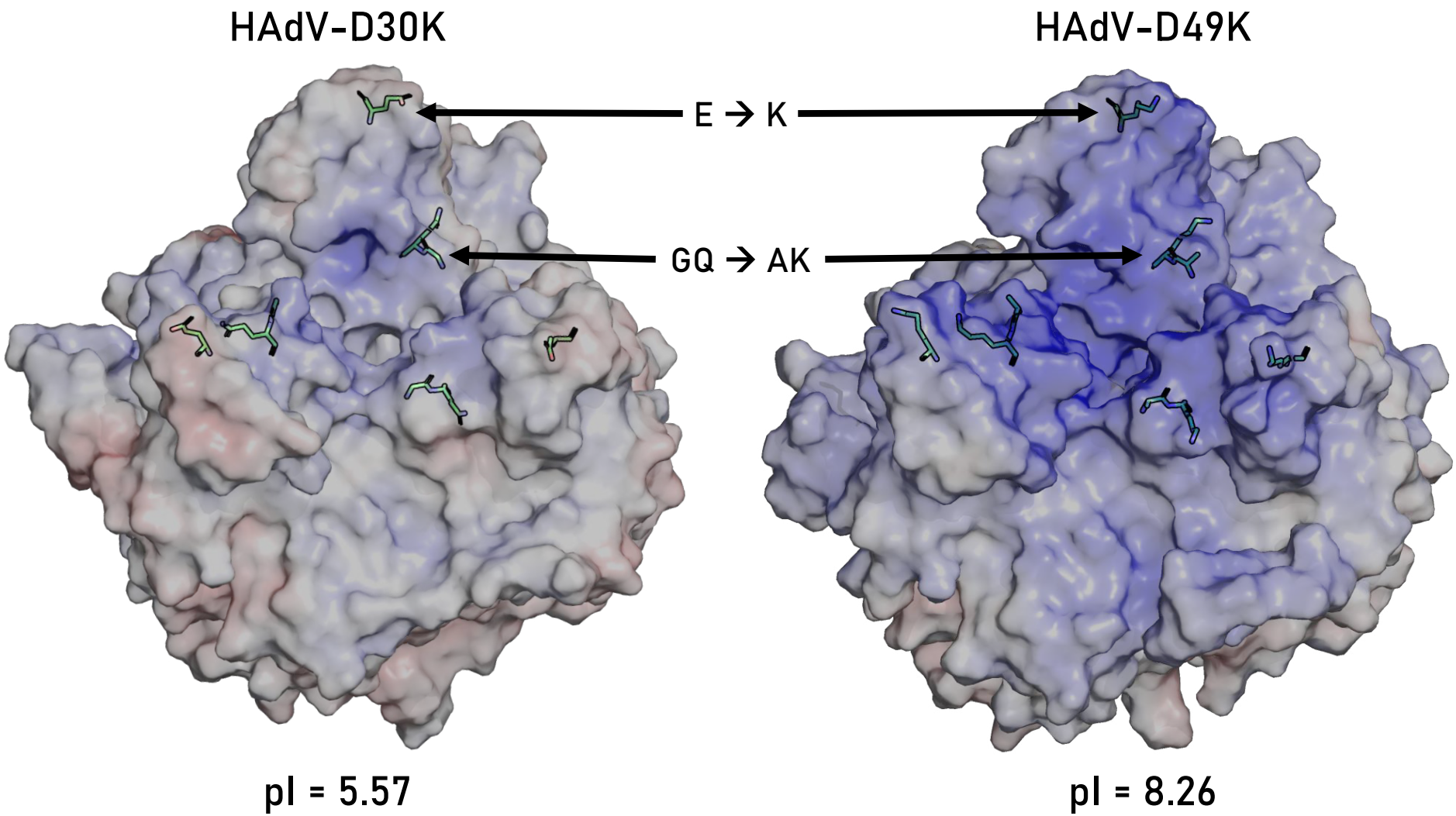

Figure 5

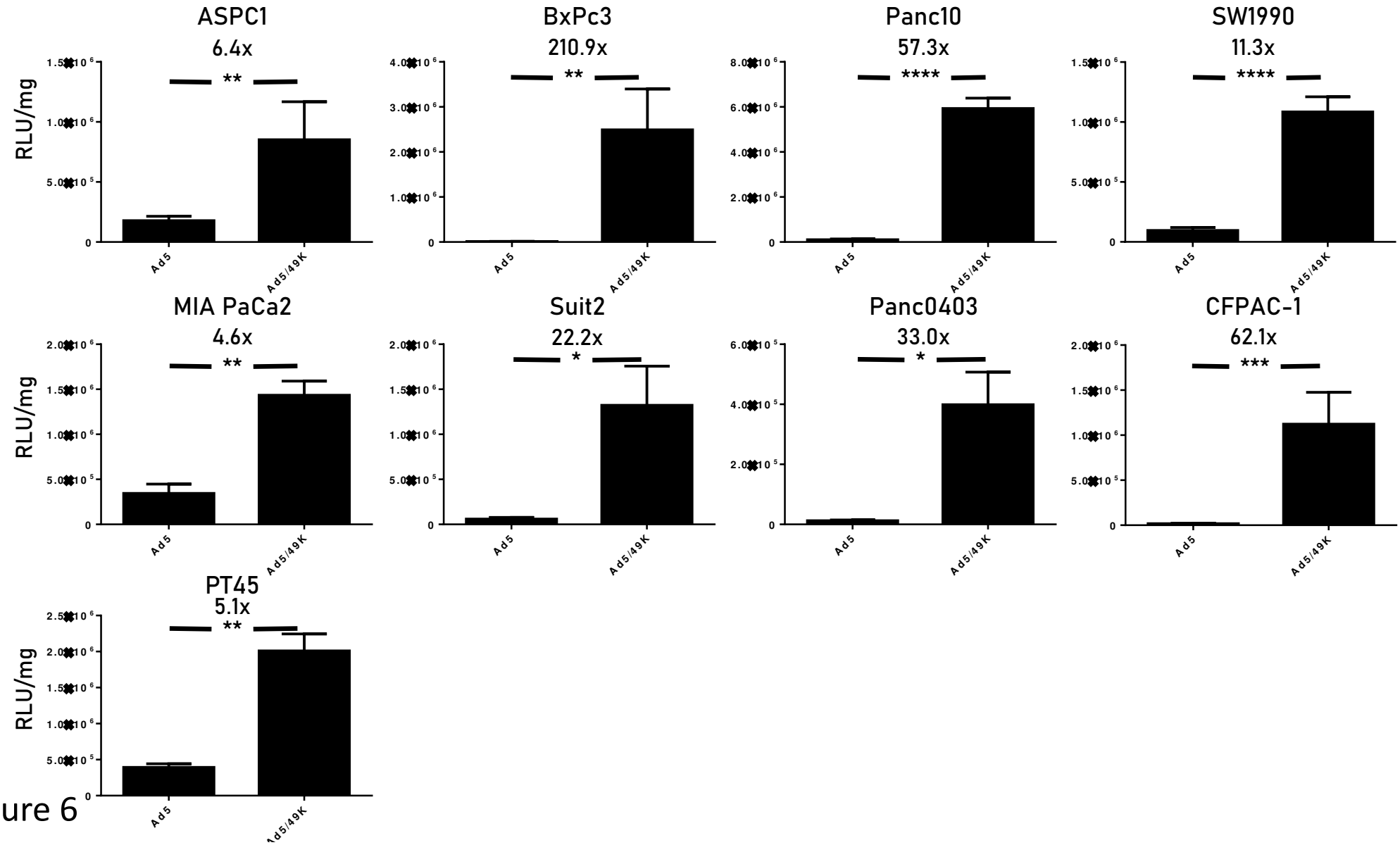
ASPC1
6.4x
**
BxPc3
210.9x
**
Panc10
57.3x
****
SW1990
11.3x
****
MIA PaCa2
4.6x
**
Suit2
22.2x
*
Panc0403
33.0x
*
CFPAC-1
62.1x
***
PT45
5.1x
**
RLU/mg
Ad5
Ad5/49K

Figure 6

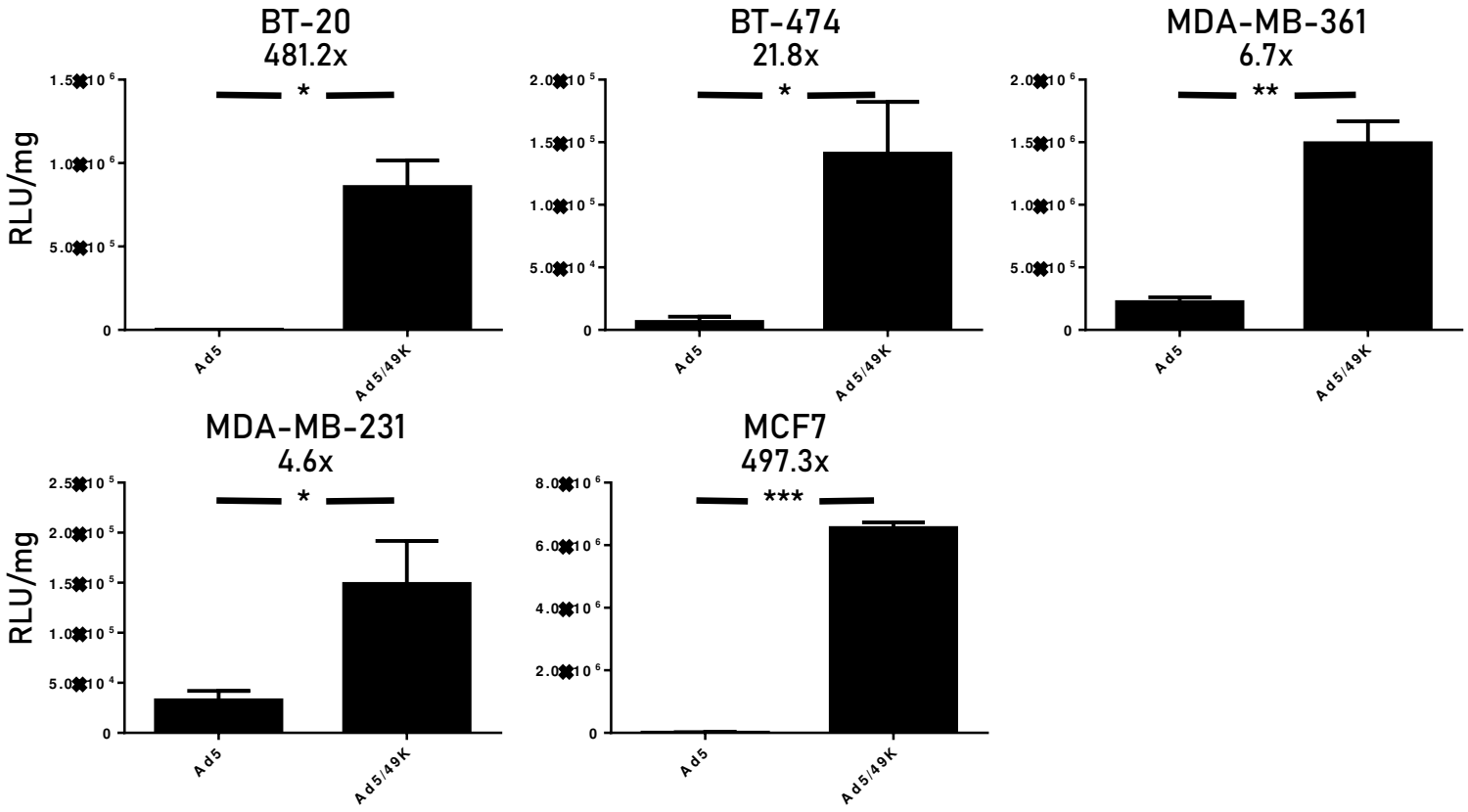
BT-20
481.2x
*
BT-474
21.8x
*
MDA-MB-361
6.7x
**
MDA-MB-231
4.6x
*
MCF7
497.3x
***
RLU/mg
Ad5
Ad5/49K

Figure 7

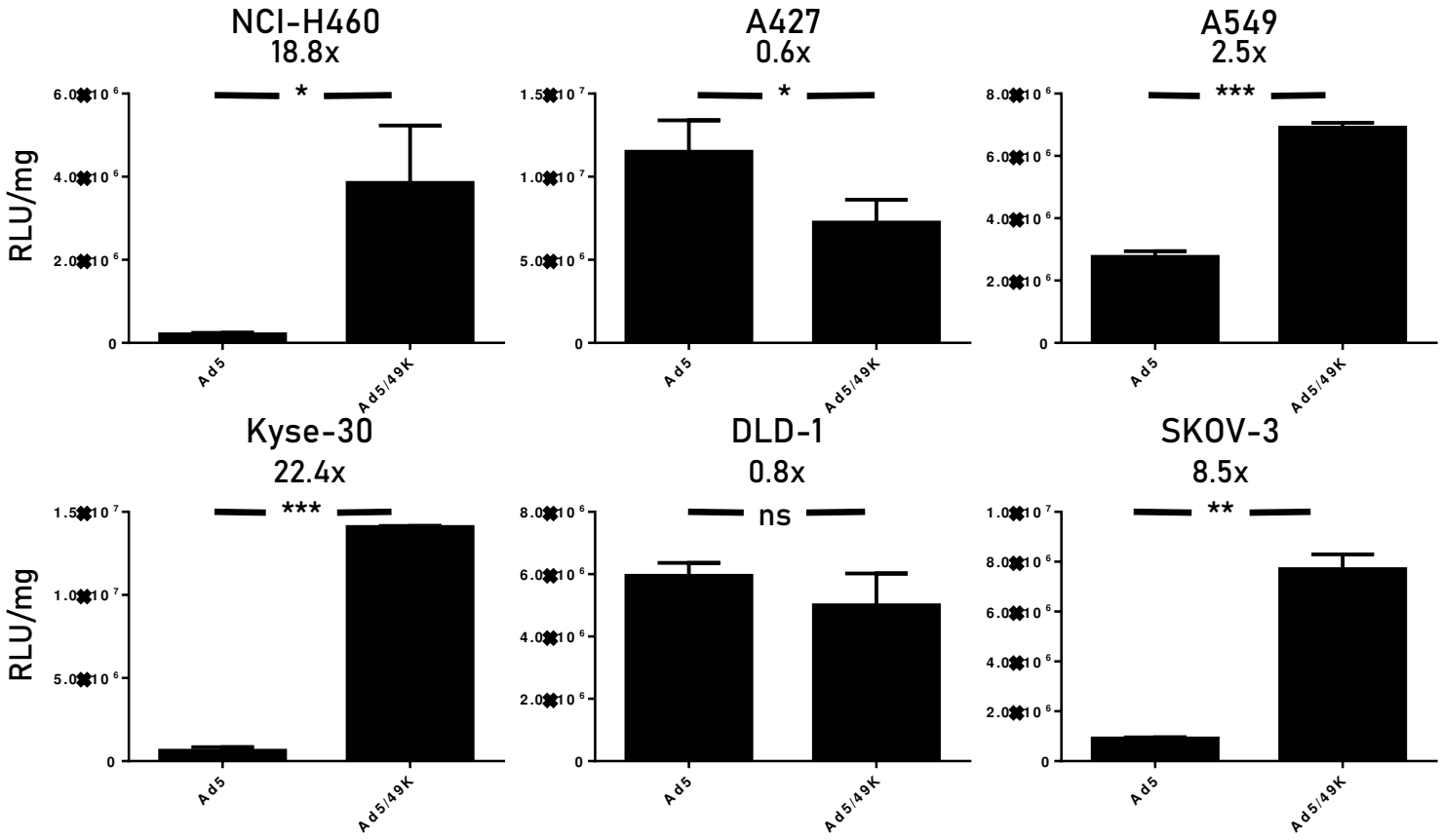
NCI-H460
18.8x
A427
0.6x
A549
2.5x
Kyse-30
22.4x
DLD-1
0.8x
SKOV-3
8.5x
RLU/mg
*
*
***
***
ns
**
Ad5
Ad5/49K

Figure 8